Available online at www.sciencedirect.com
SCIENCE DIRECT®
Journal of the European Ceramic Society 25 (2005) 3269–3279
www.elsevier.com/locate/jeurceramsoc

# Synthesis of $CaAl_2O_4$ from powders: Particle size effect

J.M. Rivas Mercury[1], A.H. De Aza, P. Pena*

*Instituto de Cerámica y Vidrio, CSIC, Camino de Valdelatas s/n 28049, Cantoblanco, Madrid, Spain*

Received 3 April 2004; received in revised form 21 June 2004; accepted 26 June 2004
Available online 10 November 2004

**Abstract**

Starting from high energetic attrition milled mixtures of either $\alpha$-$Al_2O_3$ or amorphous ($Al(OH)_3$) with $CaCO_3$ the binary compound calcium monoaluminate ($CaAl_2O_4$) was synthesized with high purity. The processes were carried out on samples with the nominal $CaAl_2O_4$ stoichiometry. High energetic attrition milling of the reactants does not eliminate the starting carbonate, both batches showed a high degree of homogeneity and they behaved similarly on heating, forming $CaAl_2O_4$ at temperatures lower than 1300 °C. These temperatures are lower than that required for the traditional solid state reaction process. The $CaAl_2O_4$ synthesis path implies the formation of cryptocrystalline and crystalline $Al_2O_3$, CaO, $Ca_{12}Al_{14}O_{33}$ and $CaAl_4O_7$ as transitory phases. The nucleation and growth of $CaAl_2O_4$ took place at 1300 °C and shows a porous structure and small grain size (∼1.5 μm).


*Keywords:* $CaAl_2O_4$; Milling synthesis; Solid state reactions; Processing

## 1. Introduction

Calcium monoaluminate, $CaAl_2O_4$, is a refractory compound located in the $Al_2O_3$–CaO binary system[1] that melts congruently at 1600 °C.[1] $CaAl_2O_4$ is the majority component, and the main responsible for the hydraulic hardening, of high alumina cements. In recent years, calcium aluminates based materials have found new applications in the field of advanced ceramics as optical ceramics,[2] catalyst support,[3] flame detectors,[4,5] dental cements[6] and structural ceramics.[7]

When $CaAl_2O_4$ is prepared by conventional methods the final product of solid-state reactions may contain phases like CaO, $CaAl_4O_7$ and $Ca_{12}Al_{14}O_{33}$ as main impurities below 1300 °C.[8,9] Hence, successful preparations of $CaAl_2O_4$ by solid state reaction required multiple milling and high-temperature firings (above 1550 °C). Nowadays, it is possible to decrease the synthesis temperature of inorganic compounds through sol–gel methods,[2,10] polymerisation of organic solutions (Pechini method),[3,11] combustion synthesis method,[12,13] high energetic attrition milling and mechanochemical treatments (especially if at least one component contains carbonate or hydroxyl groups).[14] The last aforementioned synthesis route is described as a "*soft*" mechanochemical method.[15] The use of mixtures that contains carbonates and/or hydroxides is an attractive alternative to produce low cost calcium aluminates.[7]

This paper deals with the reaction sintering mechanism of $CaAl_2O_4$ formation by means of high energetic attrition milled mixtures of either $\alpha$-$Al_2O_3$ or amorphous $Al(OH)_3$ with $CaCO_3$.

## 2. Experimental procedure

The starting materials used in this investigation were: alumina CT 3000 SG (Alcoa, Pittsburgh, PA, USA), analytical grade $Al(OH)_3$ (Alfa Aesar, Jonhson Matthey, Germany) and $CaCO_3$, calcite (Merck, Germany). Table 1 shows the

* Corresponding author.
*E-mail address:* Ppena@icv.es (P. Pena).
[1] Present address: Centro Federal de Educação Tecnológica do Maranhão, CEFET-MA Av. Getúlio Vargas, 04, Monte Castelo, CEP 65025-001, São Luís, MA, Brasil.

0955-2219/$ – see front matter © 2004 Published by Elsevier Ltd.
doi:10.1016/j.jeurceramsoc.2004.06.021

Table 1
Physical characteristics and chemical analysis of raw materials

| Analytical method | $CaCO_3$ | $Al(OH)_3$ | $\alpha$-$Al_2O_3$ |
|---|---|---|---|
| Chemical analysis (wt.%) | | | |
| Ignition loss | 43.75 | 46.00 | 0.045 |
| $SiO_2$ | –[a] | 0.25 | 0.08 |
| $TiO_2$ | –[a] | 0.01 | 0.005 |
| $Al_2O_3$ | 0.009 | 53.4 | 99.6 |
| CaO | 55.8 | 0.12 | 0.02 |
| MgO | 0.08 | 0.02 | 0.1 |
| $Na_2O$ | <0.20 | <0.2 | 0.1 |
| $K_2O$ | 0.012 | 0.01 | 0.002 |
| $Fe_2O_3$ | 0.0007 | 0.01 | 0.04 |
| $SO_4$ | 0.01 | –[a] | –[a] |
| | Calcite | Amorphous | $\alpha$-$Al_2O_3$ |
| Mineralogical analysis | | | |
| Specific surface[b] BET ($m^2\,g^{-1}$) | 0.20 | 39.0 | 8.00 |
| Particle size $d_{50}$ ($\mu$m) | 13.80 | 6.25 | 0.38 |
| Real density[c] ($g\,cm^{-3}$) | 2.69 | 2.20 | 3.93 |

[a] Undetermined.
[b] BET.
[c] Helium picnometry.

chemical analysis and physical characteristics of these raw materials.

Two mixtures of either $\alpha$-$Al_2O_3$ or amorphous $Al(OH)_3$ with $CaCO_3$ with compositions according to the stoichiometric proportions of Eqs. (1) and (2) were prepared. They will be referred through this paper as CA and CAG, respectively.

$$CaCO_3 + Al_2O_3 \rightarrow CaAl_2O_4 + CO_2(g)\ (CA) \quad (1)$$

$$CaCO_3 + 2Al(OH)_3 \rightarrow CaAl_2O_4 + 3H_2O(g) + CO_2(g)\ (CAG) \quad (2)$$

Concerning the first case (1), a 50 wt.% solids aqueous suspension of $CaCO_3$/$\alpha$-$Al_2O_3$ mixture was prepared. To provide maximum stability to the suspension 0.8 wt.% Dolapix-CE 64 (Zschimmer & Schwarz, Lanstein, Germany) and 0.1 wt.% Trimetil Hydroxyl Ammonium (HTMA) were added. These last mentioned percentages are related to the solids content. To obtain a homogeneous and high energetic attrition milled batch, the mixture was wet ground in a laboratory scale annular gap mill[16] with high-purity 3 mm alumina balls. 180 $cm^3$ of alumina balls were used to have a balls/powder weight ratio of 5/1. The unit can be loaded continuously and the milling process consisted on passing the powder suspension through the mill chamber that contains the alumina balls several times. The residence time of the power suspension in the milling chamber is ~15 min/cycle. After each milling cycle, the particle/agglomerate size distribution was measured by laser diffractometry (Mastersizer, Malvern Instrument, UK) to select the optimum milling time.

As mentioned before a $CaCO_3$/$Al(OH)_3$ batch was also processed. In this case the powder mixture (2) was wet ground in a closed chamber laboratory attrition mill using high-purity 1 mm magnesia partially stabilized zirconia balls (Mg-PSZ) as grinding media and isopropyl alcohol as suspension media. A ball/powder weight ratio of 5/1 was used. In this case the particle/agglomerate size distribution was measured after different grinding times by laser diffractometry to select the optimum milling time.

The mill choice was taken bearing in mind the starting mixture quantity: 1000 g in the case of $CaCO_3$/$\alpha$-$Al_2O_3$ mixture and 100 g in the case of $CaCO_3$/$Al(OH)_3$ batch. The grinding media, either $Al_2O_3$ or Mg-PSZ balls, was changed from one batch to another due to the alumina balls shock-wear detected after the first mixture was processed. Then, Mg-PSZ balls were selected to process the $CaCO_3$/$Al(OH)_3$ mixture due to its better tribology.

After milling, the batches were spray-dried (Lab Plant, SD-05) and cold isostatically pressed at 50 MPa, to produce cylindrical green compacts of about 10 mm diameter.

Differential thermal analysis and thermogravimetry (DTA and TG, Netzch STA 409, Germany) studies were conducted, in air, on green compacted samples at a constant heating rate of 5 °C $min^{-1}$ up to 1450 °C using Pt crucibles. Dilatometric analysis (Setaram Setsys 16/18 with $\alpha$-alumina support, France) and X-ray diffraction (XRD, Siemens D-5000, Kristalloflex 710, with Cu K$\alpha_{1,2}$ and secondary curved graphite monochromator, Germany) were used to study the reaction-sintering process up to 1550 °C. The dilatometric studies were conducted at heating rate of 5 °C $min^{-1}$ on specimens of 20 mm length.

Additionally, isothermal treatments were performed in an electrical furnace with 1700 °C Super-Kanthal heating elements (Switzerland) at temperatures from 800 °C to 1400 °C during 1 min. A heating and cooling rate of 5 °C $min^{-1}$ was used. The phase composition of the obtained compacts was determined by XRD.

Microstructural analysis and phase identification, of the obtained materials, was carried out by scanning electron microscopy (SEM) using a C. Zeiss DSM 950 SEM (Germany) fitted with an energy dispersive spectrometer (EDS, Tracor Northern), on either polished and thermally etched samples or fractured surfaces, coated with gold by sputtering.

To support the reaction mechanism proposed, thermodynamic calculations of the Gibbs energy were performed using the Thermo-Calc[17] computation package. This software offers an exhaustive thermochemical database which includes enthalpy (H), entropy (S) and heat capacity (C) data for chemical compounds.

## 3. Results

### 3.1. Effect of grinding on the particle size and structure of the $CaAl_2O_4$ precursors

The particle size distributions of $CaCO_3$/$\alpha$-$Al_2O_3$ powder mixture, at the 1:1 molar ratio, after 1 and 9 milling cycles (namely CA1 and CA9) were bimodal and the maximums are centered on 0.35 and 2 $\mu$m, respectively (Fig. 1a and b).

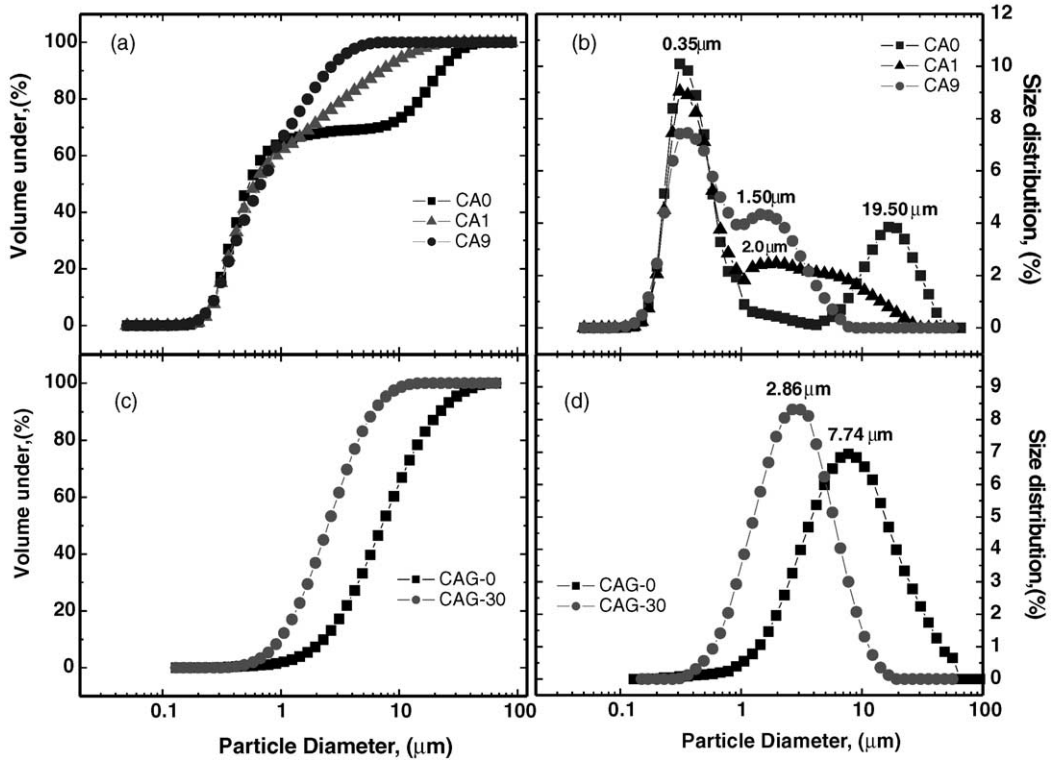


Fig. 1. (a–d) Particle size distributions of powder mixtures after milling. (a and b) $CaCO_3/\alpha$-$Al_2O_3$ batch. (c and d) $CaCO_3$–$Al(OH)_3$ mixture.

The maximum located at ≈0.35 μm corresponds to the α-$Al_2O_3$ powder and the one placed at about 2 μm is attributed to $CaCO_3$ particles (Table 1). As shown in Table 2, the average particle/agglomerate size values, $d_{50}$, changed slightly with milling time from 0.60 to 0.56 μm. Otherwise, the maximum size of the 90 wt.% of the particles, $d_{90}$, were strongly dependent on the milling process and decreased from 7.10 to 2.96 μm. This latter parameter determines the reaction capability of the compacted powders. From the milling behavior it is deduced that the $CaCO_3$, that presented some hard agglomerates above 40 μm, has reduced its average size to values smaller than 10 μm (see Fig. 1b). Its initial specific surface area was 5.6 $m^2\,g^{-1}$ which rises up to 8.0 $m^2\,g^{-1}$ after the attrition milling.

Table 2
Physical characteristics of powders after milling

| Analytical method | CA1 | CA9 | CAG-0 | CAG-30 |
|---|---|---|---|---|
| Chemical analysis (wt.%) | | | | |
| Ignition loss | 23.65 | 22.50 | 45.40 | 45.46 |
| $Na_2O$ | 0.03 | 0.03 | 0.2 | 0.2 |
| CaO | 27.80 | 27.50 | 21.73 | 21.73 |
| $Al_2O_3$ | 48.35 | 49.85 | 39.68 | 39.68 |
| $K_2O$ | 0.005 | 0.005 | 0.001 | 0.001 |
| MgO | 0.05 | 0.05 | 0.04 | 0.04 |
| $SiO_2$ | 0.15 | 0.15 | 0.15 | 0.15 |
| Particle size $d_{50}$ (μm) | 7.10 | 2.96 | 21.95 | 5.68 |
| Particle size $d_{50}$ (μm) | 0.60 | 0.56 | 7.15 | 2.19 |
| Specific surface[a] ($m^2\,g^{-1}$) | 5.60 | 8.00 | 22.00 | 27.00 |
| Real density[b] ($g\,cm^{-3}$) | 2.19 | 2.23 | 2.31 | 2.34 |

[a] BET.
[b] Helium picnometry.

The α-$Al_2O_3$ weight content in the CA composition (1) slightly increases with milling time from 63.5 to 65.4% (Table 2) due to the, above mentioned, alumina release from the grinding media. This fact, as is discussed later on, is considered to have a positive effect on the results.

As it is shown in Table 2 and Fig. 1c and d, the particle size distributions of $CaCO_3/2Al(OH)_3$ powder mixture at the beginning of the process (CAG-0) and after 30 min of milling (CAG-30) were monomodal with the maximums centered on 7.74 and 2.86 μm, respectively (Fig. 1d). The maximum size of the 90 wt.% of the particles, $d_{90}$, was also strongly dependent on the milling process and decreased from 21.95 to 5.68 μm. In this case, the specific surface area increases with the milling process from 22 to 27 $m^2\,g^{-1}$ (Table 2).

Fig. 2a and d shows the XRD patterns of the unground and ground mixtures. Differences between the diffractograms of the original and the mechanically treated samples indicated that calcite suffers significant structural degradation (Fig. 2a and b). The distortion of the structure induced by grinding in CAG batch is reflected in the line boardening and shift in reflections, as well as the reduction of peak intensities (areas). Recently, it was shown that this X-ray line boardening is mainly due to lattice microstrains, rather than microcrystalline size.[18]

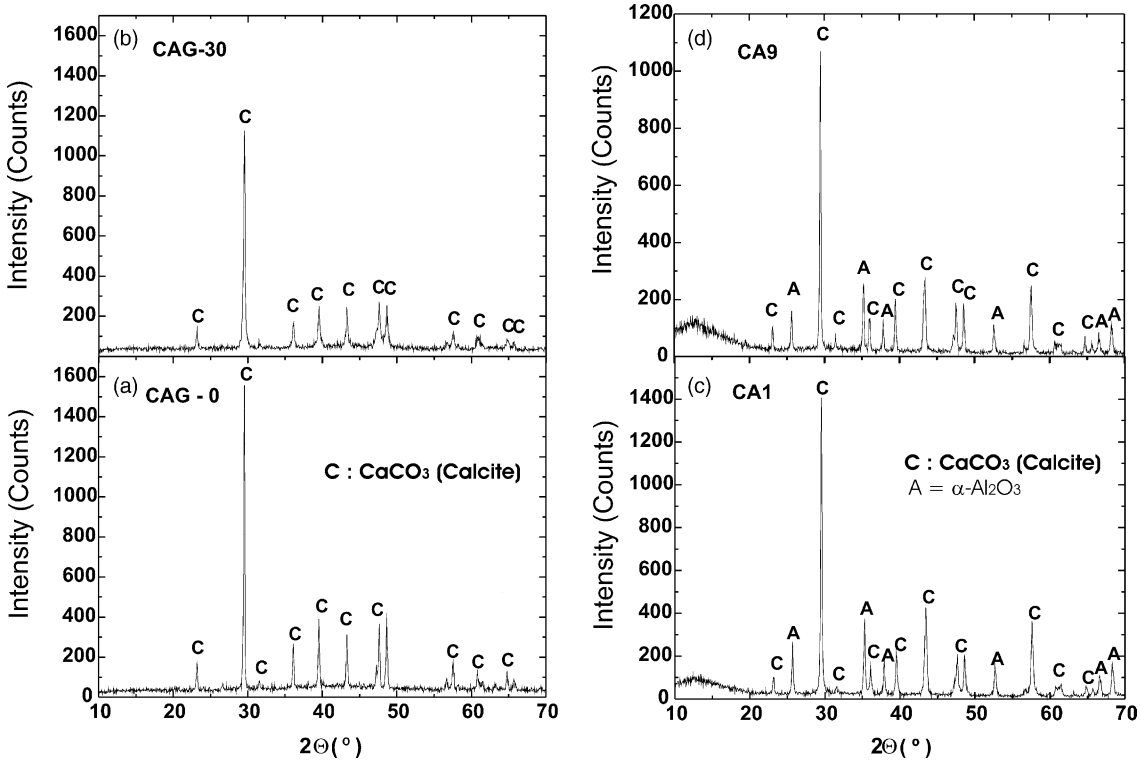


Fig. 2. (a–d) XRD patterns of unground and ground starting mixtures. (a and b) $CaCO_3$–$Al(OH)_3$ mixture. (c and d) $CaCO_3$/α-$Al_2O_3$ batch.

### 3.2. Non-isothermal study of the reaction process

When the $CaCO_3/Al_2O_3$ and $CaCO_3/2Al(OH)_3$ mixtures were subjected to thermal treatment at a constant heating rate, several phenomena were observed by DTA, TG, dilatometry and XRD.

The thermal evolution, DTA and TG plots, of the CA1 and CA9 mixtures are shown in Fig. 3a and b. Both samples experienced significant weight loss of 23.41 and 22.89 wt.%, respectively. These are related with the endothermic peaks registered at ≈845 °C and 852 °C for CA1 and CA9, respectively. These effects are attributed to $CO_2$ release.[19] The exothermic peaks registered at ≈250 °C are related to the combustion of the reological additives used, that are physically adsorbed on the particles surface. Both samples showed sharp exothermic peaks at 928 °C and 917 °C, respectively and broad exothermic effects at about 1088 °C, attributed to calcium aluminates formation: $Ca_{12}Al_{14}O_{33}$ and $CaAl_2O_4$, respectively.

The ATD and TG recorded curves for the CAG-30 mixture are shown in Fig. 4a. This mixture presents a significant weight loss of ≈45.46% in two separated stages (≈25% and ≈20.46 wt.%, respectively). These stages matched with two endothermic effects. The first one, very broad with its minimum at ≈141 °C is assigned to the dehydration of the amorphous aluminum hydroxide used, and the second one with its minimum at ≈757 °C to the carbonate decomposition. The exothermic peak registered at ≈427 °C is due to the combustion of residual isopropyl alcohol, used as suspension media for the milling process, physically adsorbed on the particles surface. The exothermic effects registered at ≈920 °C and ≈1080 °C are attributed to calcium aluminates formation: $Ca_{12}Al_{14}O_{33}$ and $CaAl_2O_4$, respectively.

The constant heating rate dilatometric curves registered for the green compacts of CA1 and CA9 samples are shown in Fig. 3c and d. Both samples show between 815 °C and 1280 °C a significant expansion attributed to the formation of calcium aluminates, mainly $CaAl_2O_4$ ($\Delta V$ = 24.19%). At temperatures higher than 1200 °C, the predominant effect is shrinkage. The CA1 sample shows again an expansive effect at about ∼1.420 °C.

The constant heating rate dilatometric study for CAG-30 sample is shown in Fig. 4b. This sample show four shrinkage effects at ∼141 °C, ∼838 °C, ∼906 °C, and ∼1280 °C and three expansive effects at ∼325 °C, ∼850 °C and ∼920 °C, attributed to the decomposition of $Al(OH)_3$ and $CaCO_3$ and calcium aluminates formation, respectively.

In Fig. 5, the variation of apparent density versus temperature of CA1, CA9 and CG-30 compacted samples is represented. CA1 and CA9 densities were practically the same up to ∼800 °C (2.01 and 2.03 g cm$^{-3}$) but then diverged. The density of CA1 decreased from ∼750 °C up to 1200 °C and then increased rapidly. This compact has a density of $\rho/\rho_{th}$ = 89.93% at ∼1400 °C. The density of CA9 decreased from ∼750 °C to 1150 °C and then increased rapidly up to ∼1400 °C, reaching a final density of $\rho/\rho_{th}$ = 93.29%. On the other hand, the density of the sample CAG-30 presents a different behavior. At low temperatures a small decrease

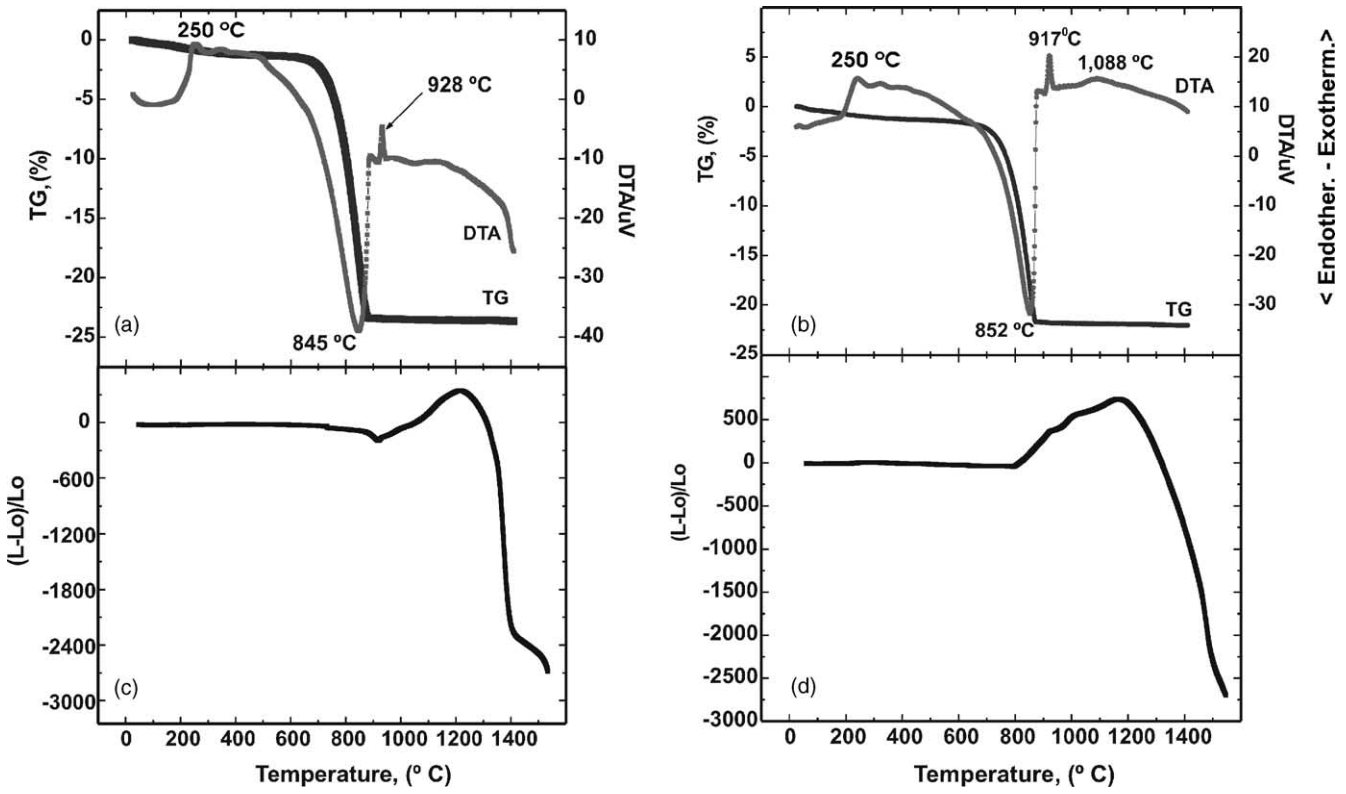


Fig. 3. (a and b) Thermal evolution of $CaCO_3/\alpha$-$Al_2O_3$ green compacted samples. DTA and TG plots registered at heating rate of 5 °C $min^{-1}$. (a) CA1 sample, namely after one milling cycle, and (b) CA9 sample, that is after nine milling cycles. (c and d) Constant heating rate dilatometry curves registered at heating rate of 5 °C $min^{-1}$ for the green compacts of samples. (c) CA1 and (d) CA9 sample.

of the density can be observed, which reaches a minimum at 170 °C; from this temperature up to 600 °C a small increment is registered and from this point up to 800 °C a new decrease in density can be seen. Finally from 800 °C to 1400 °C density increases slowly, reaching a final density of $\rho/\rho_{th} = \sim 60\%$.

The crystalline phases identified in the CA1, CA9, and CAG-30 compacted and heat treated samples at different temperatures are summarized in Tables 3 and 4. In all the samples the reaction was complete at 1300 °C. It is worth to mention that during the reaction process the phases $Ca_3Al_2O_6$ and $CaAl_{12}O_{19}$ were not detected in any of the studied samples. The intermediate phase $Ca_{12}Al_{14}O_{33}$, was present in all the samples treated at temperatures between 900 °C and 1200 °C. Furthermore, the presence of $CaAl_4O_7$ was also detected as a transitory phase in the CAG sample.

Table 3
Phases identified by XRD analysis after 1 min annealing at different temperatures of $CaCO_3/\alpha$-$Al_2O_3$ samples

| Temperature | $CaCO_3$ | CaO | $Ca_{12}Al_{14}O_{33}$ | $CaA_{l2}O_4$ | $CaA_{l4}O_7$ | $\alpha$-$Al_2O_3$ |
|---|---|---|---|---|---|---|
| CA1/RT | +++ | – | – | – | – | +++ |
| CA1/900 °C | – | +++ | ++ | – | – | ++ |
| CA1/1100 °C | – | – | ++ | +++ | – | ++ |
| CA1/1200 °C | – | – | ++ | +++ | – | – |
| CA1/1300 °C | – | – | ++ | +++ | – | – |
| CA1/1400 °C | – | – | + | +++ | – | – |
| CA1/1550 °C | – | – | + | +++ | – | – |
| CA9/RT | +++ | – | – | – | – | +++ |
| CA9/900 °C | – | +++ | + | – | – | +++ |
| CA9/1100 °C | – | – | ++ | ++ | – | +++ |
| CA9/1200 °C | – | – | ++ | +++ | ++ | ++ |
| CA9/1300 °C | – | – | – | +++ | + | – |
| CA9/1400 °C | – | – | – | +++ | + | – |
| CA9/1550 °C | – | – | – | +++ | + | – |

+++, majority phases; ++, abundant phases; +, minority phases.

Table 4
Phases identified by XRD analysis after 1 min annealing at different temperatures of $CaCO_3/Al(OH)_3$ samples

| Temperature | $CaCO_3$ | $Al(OH)_3$ | CaO | $Ca_{12}Al_{14}O_{33}$ | $CaAl_2O_4$ | $CaAl_4O_7$ | $\alpha$-$Al_2O_3$ |
|---|---|---|---|---|---|---|---|
| CAG-30/RT | +++ | +++ | – | – | – | – | – |
| CAG-30/900 °C | – | – | +++ | ++ | +++ | – | – |
| CAG-30/1100 °C | – | – | – | ++ | +++ | + | ++ |
| CAG-30/1200 °C | – | – | – | ++ | +++ | – | – |
| CAG-30/1300 °C | – | – | – | – | +++ | – | – |

+++, majority phases; ++, abundant phases; +, minority phases.

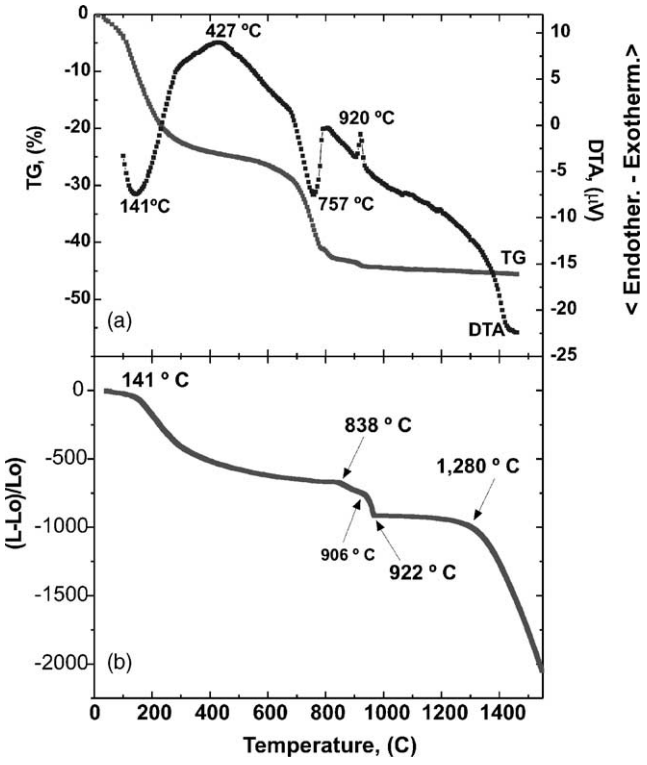


Fig. 4. (a and b) Thermal evolution of CAG-30 green compacted sample, that is $CaCO_3/Al(OH)_3$ batch. (a) DTA and TG plots registered at heating rate of 5 °C $min^{-1}$. (b) Constant heating rate dilatometry curve registered at heating rate of 5 °C $min^{-1}$.

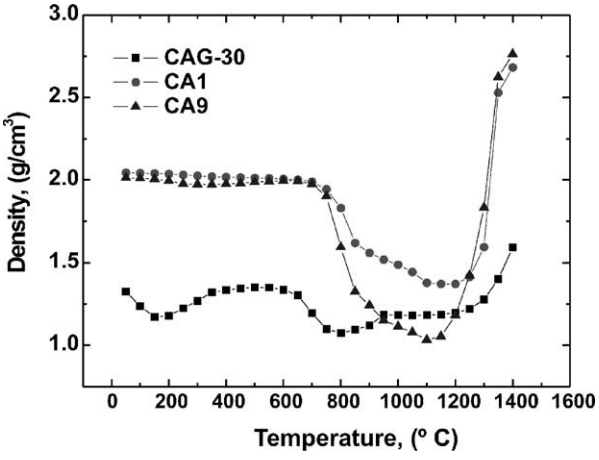


Fig. 5. Variation of apparent density vs. temperature of the CA1, CA9 and CAG-30 compacts.

### 3.3. Microstructure development

#### 3.3.1. Fractured surfaces

The microstructure evolution with temperature was studied by scanning electron microscopy in samples treated at 1000 °C, 1300 °C and 1400 °C during 1 min and subsequently quenched. Samples heated at lower temperatures were not suitable for study due to the high reactivity of the free CaO.

Fig. 6a and b shows typical SEM images of fractured surfaces of the CA1 and CA9 samples, heated at 1000 °C during 1 min. The samples show a high density of small pores and the crystalline phases show a small grain size (<500 nm). In these figures, clusters made up of CaO particles can be clearly distinguished. These clusters have around ∼7 μm and have been formed from the coarse $CaCO_3$ particles present in the green compacted samples. Gaps between these clusters and the finest fraction of the sample are also detected. At this temperature neck formation between the finest particles is beginning induced by sintering. It is worth to stand out that in CA9 sample some $\alpha$-$Al_2O_3$ particles of ∼5 μm coming from the wear of the grinding media are also detected (Fig. 7b).

The microstructures of samples CA1 and CA9 treated at 1400 °C are shown in Fig. 6c and d. These samples show a significant sintering rate and an increased pore and grain size, ∼2 and 1 μm, respectively. The neck formation between particles is evident and the formation of pore channels by coalescence of small particles is also clearly observed. In none of the samples treated at 1400 °C the presence of CaO-rich secondary phases or segregations were detected by SEM-EDS.

Fig. 7a shows typical SEM images of fractured surfaces of the CAG-30 sample heated at 1000 °C for 1 min. This sample shows a high density of small pores (<500 nm). The crystalline phases also show a small grain size (<500 nm). The presence of clusters of 8 μm, made up of CaO particles, can be clearly distinguished. Gaps between these clusters and the finest fraction of the sample are also detected in this case. Fig. 7b shows the typical microstructure of a CAG-30 sample heat treated at 1300 °C, which corresponds to a fine grained porous monophasic compact. The $CaAl_2O_4$ particles show a ∼1.5 μm grain size. It can be seen that the neck formation between the finest particles is beginning.

#### 3.3.2. Polished surfaces

Polished and thermally etched surfaces of CA1 and CA9 samples treated at 1550 °C were studied by SEM-EDS (Fig. 8).

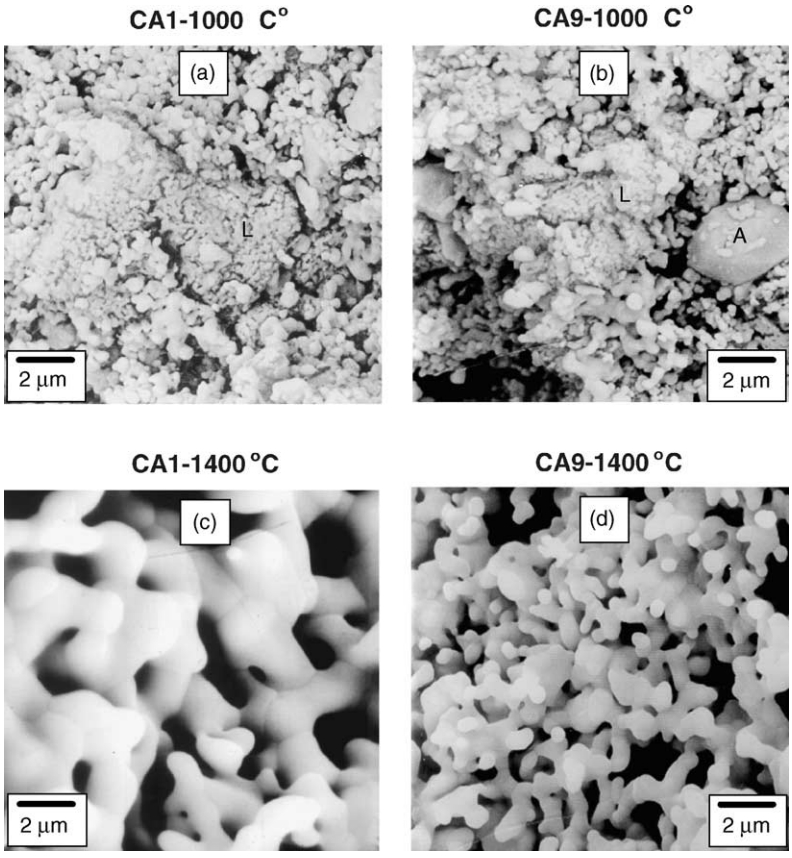


Fig. 6. SEM micrographs of the fracture surfaces of $CaCO_3/\alpha$-$Al_2O_3$ compacts treated at different temperatures. Back scattered electron images. (a) CA1 sample treated at 1000 °C during 1 min showing clusters made up of CaO particles (L). These clusters have been formed from the coarse $CaCO_3$ particles present in the green compacted samples. (b) CA9 sample 1 min heated at 1000 °C showing the presence of CaO clusters and some fragment of alumina (A) coming from the grinding media wear. (c and d) CA1 and CA9 samples treated at 1400 °C showing a porous and fine grained microstructure made up of $CaAl_2O_4$. Neck formation between the finest particles is beginning induced by sintering.

In CA1 sample a high grain growth rate of the phase $CaAl_2O_4$ is observed and a significant quantity of liquid phase is also detected (Fig. 8a).

Additionally, in CA9 sample large pores were observed. In Fig. 8b it can be seen $CaAl_4O_7$ dark gray grains, as it has been confirmed by SEM-EDS, with an average size of ~2 μm.

From the microstructural examination and the XRD analysis, Table 3, it can be concluded that in all the studied samples the reaction process is ended at 1300 °C but the sintering process is not completed yet.

## 4. Discussion

The initial powder mixtures were constituted by hard coarse $CaCO_3$ particles and either fine $\alpha$-$Al_2O_3$ particles or amorphous aluminum hydroxide agglomerates, which were easily broken during the initial stages of milling (Tables 1 and 2, and Fig. 1). The specific surface area of the $CaCO_3/\alpha$-$Al_2O_3$ batch increased ~42.86% with milling, however $CaCO_3/Al(OH)_3$ mixture show an increase in specific surface area around of 23% with milling process.

The increase in the specific surface area, the reduction in grain size and the decrease in the crystallinity of particles, facilitates the reaction process and minimize the possibility of forming chemical segregations, as observed by other workers when the reaction sintering of samples with coarse grains of calcite[20] was studied.

The total loss of weight due to decomposition of reactants during the thermal treatment was calculated with the equation,

$$\Delta W = \Sigma f_i \cdot \Delta W_i \quad (3)$$

where $f_i$ and $\Delta W_i$ are the weight fraction and weight loss, respectively, for every reactant. Using the weight loss data of reactants, shown in Table 1, it is possible to establish theoretical losses of 28.03% for the hydroxide and 15.78% for the carbonate in CAG-30 sample. If we compared these values with the ones found from thermogravimetry (Fig. 4), we can easily relate the first observed loss up to 650 °C to the dehydration of aluminum hydroxide (28.03%) and the second, between 700 °C and 1200 °C, of 17.66% to calcite decomposition. If the global loss (encompassing the decomposition of both reactants) is considered, the slight discrepancy between the theoretical (43.81%) and the observed (45.46%) is due to

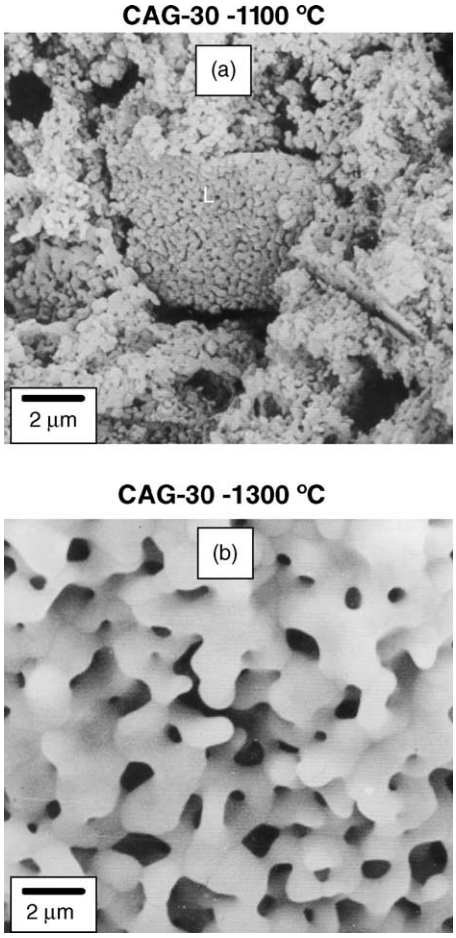


Fig. 7. (a) Typical SEM images of fractured surfaces of the CAG-30 sample heated at 1000 °C for 1 min. The presence of clusters made up of CaO particles (L) can be clearly distinguished. (b) The typical microstructure of a CAG-30 sample heat treated at 1300 °C, which corresponds to a fine grained porous monophasic compact of $CaAl_2O_4$. It can be seen that the neck formation between the finest particles is beginning.

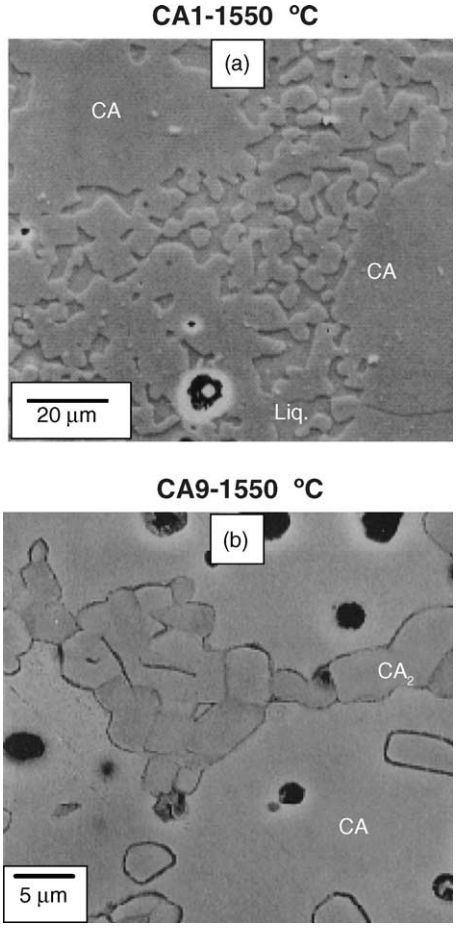


Fig. 8. Typical microstuctures of polished and thermally etched surfaces of CA1 and CA9 samples treated at 1550 °C. (a) CA1 sample with a high grain growth rate of the $CaAl_2O_4$ phase and a significant quantity of glassy phase. $Ca_{12}Al_{17}O_{33}$ was detected by XRD and SEM-EDS on this sample as a phase that has been devitrified from the liquid phase during the cooling process. (b) CA9 sample with large pores and $CaAl_4O_7$ dark gray grains and small quantities of $CaAl_4O_7$. See text for details.

the volatilisation of the remaining isopropanol adsorbed on the surface of the powder (1.65%). In fact, the wide exothermic peak registered at ≈427 °C is due to the combustion of residual organic products.

On the other hand, in samples CA1 and CA9 the slight discrepancy between the theoretical loss of weight (21.78%) and the observed (23.65 and 22.50% for CA1 and CA9, respectively) is due to the evaporation of the remaining water and the combustion of the rheological additives physically adsorbed on the powder surfaces (1.87 and 0.72%). In fact, the narrow exothermic peak registered with a maximum at ∼250 °C is due to the combustion of these additives.

The results obtained by DTA and TG, the dilatometric analysis and XRD indicate that the reaction occurs before the sintering process. Therefore, it is clear that the reaction sintering process between CaO and $Al_2O_3$ proceeds in two well separated steps: (a) reaction and (b) sintering of the products. This fact is in close agreement with the works of Ali et al.,[21] Singh and Mandal,[20] Rivas Mercury et al.[22] and De Aza et al.[23] Evidence arisen from experimental data allows the different phase transitions, or reactions, to be distinguished.

### 4.1. Reaction process

Considering the Gibbs energy ($\Delta G$) of the possible reactions involved in the calcium aluminates formation within the binary system CaO–$Al_2O_3$ (Table 5), together with the thermal analyses, the studied sintering behavior (Figs. 3–5) and the crystalline phases identified by XRD and SEM-EDS (Tables 3 and 4 and Figs. 6–8), the following reaction mechanism is proposed.

#### 4.1.1. $CaCO_3$/α-$Al_2O_3$ mixtures

The solid state reaction in both $CaCO_3$/α-$Al_2O_3$ samples (CA1 and CA9) can be established as follows:

(1) The $CaCO_3$ decomposes giving up CaO (lime) in the temperature range from 600 °C to 850 °C according to

Table 5
Thermodynamic calculations of the Gibbs energy ($\Delta G$) from 25 °C to temperature indicated

| Reaction | Equation | $\Delta T$ (°C) | $\Delta G$ (kJ mol$^{-1}$) |
|---|---|---|---|
| $CaCO_3 \rightarrow CaO + CO_2(g)$ | (4) | 25–800 | 7.5 |
| $7CaAl_2O_4 + 5CaO \rightarrow Ca_{12}Al_{14}O_{33}$ | (8) | 25–1100 | −30 |
| $Al_2O_3 + CaO \rightarrow CaAl_2O_4$ | (6) | 25–900 | −38 |
| $2\alpha\text{-}Al_2O_3 + CaO \rightarrow CaAl_4O_7$ | (7) | 25–1100 | −51 |
| $5CaAl_4O_7 + Ca_{12}Al_{14}O_{33} \rightarrow 17CaAl_2O_4$ | (11) | 25–1100 | −122 |
| $Ca_{12}Al_{14}O_{33} + 5Al_2O_3 \rightarrow 12CaAl_2O_4$ | (9) | 25–1200 | −172 |
| $7Al_2O_3 + 12CaO \rightarrow Ca_{12}Al_{14}O_{33}$ | (5) | 25–900 | −275 |
| $17Al_2O_3 + Ca_{12}Al_{14}O_{33} \rightarrow 12CaAl_4O_7$ | (10) | 25–1200 | −308 |

These calculations were performed using the Thermocalc[17] computation package.

the equation:

$$CaCO_3 \rightarrow CaO + CO_2(g) \quad (4)$$

This is an endothermic reaction as the DTA clearly reveals. The loss of weight recorded in the TG plot confirms this $CO_2$ release[19] (Fig. 3a and b).

(2) At 920 °C $Ca_{12}Al_{14}O_{33}$ formation takes place by an expansive ($\Delta V$ = 36.20%) and exothermic reaction that takes place between lime and alumina (see Fig. 3a–d and Fig. 5). This transitory calcium aluminate formation is the reaction with the highest negative value of $\Delta G$ ($\Delta G_R^{900\,^\circ C} = -275\,kJ\,mol^{-1}$, Table 5).

$$7\alpha\text{-}Al_2O_3 + 12CaO \rightarrow Ca_{12}Al_{14}O_{33} \quad (5)$$

As mentioned, thermodynamic data indicate that the reaction (5) has the lowest Gibbs energy ($\Delta G$) within the system CaO–$Al_2O_3$, and therefore is viable at temperatures lower than 920 °C. However, it is obvious that the reaction does not happen until $CaCO_3$ decomposes.

(3) At $T > 1100$ °C the formation of calcium monoaluminate ($CaAl_2O_4$) takes place. It is worth to mention that in CA9 sample the formation of a second transient phase, $CaAl_4O_7$, has been detected (see Fig. 8b and Table 3). The possible reactions involved in these calcium aluminates formation are:

$$\alpha\text{-}Al_2O_3 + CaO \rightarrow CaAl_2O_4 \quad (6)$$

$$2\alpha\text{-}Al_2O_3 + CaO \rightarrow CaAl_4O_7 \quad (7)$$

$$7CaAl_2O_4 + 5CaO \rightarrow Ca_{12}Al_{14}O_{33} \quad (8)$$

$$5\alpha\text{-}Al_2O_3 + Ca_{12}Al_{14}O_{33} \rightarrow 12CaAl_2O_4 \quad (9)$$

$$17\alpha\text{-}Al_2O_3 + CaAl_{14}O_{33} \rightarrow 12CaAl_4O_7 \quad (10)$$

$$5CaAl_4O_7 + Ca_{12}Al_{14}O_{33} \rightarrow 17CaAl_2O_4 \quad (11)$$

The general features of the reaction process according to the thermodynamic calculations indicate that reaction (10) has the lowest Gibbs energy ($\Delta G$), hence it is the most favourable (Table 5) for the formation of $CaAl_4O_7$ as a transitory phase.

#### 4.1.2. $CaCO_3$/Al(OH)$_3$ mixtures

The reaction process of the CAG studied bath can be summarised as follows:

(1) The dehydration of amorphous Al(OH)$_3$ progresses quickly with the formation of cryptocrystaline $Al_2O_3$ (κ for short); these very small crystallites of $Al_2O_3$ transform to yield transition-$Al_2O_3$ in the temperature range 900–1100 °C:[24]

$$Al(OH)_3 \rightarrow \kappa\text{-}Al_2O_3 + 3H_2O(g) \quad (12)$$

$$\kappa\text{-}Al_2O_3 \rightarrow \alpha\text{-}Al_2O_3 \quad (13)$$

During heating neither boehmite nor transition-$Al_2O_3$ were detected by XRD at any temperature (100–1000 °C).

(2) The $CaCO_3$ decomposes at temperatures higher than ∼700 °C. $CaCO_3$ decomposes forming porous agglomerates or clusters made up of CaO particles according to reaction (4) (Fig. 4 and Fig. 7a).

(3) The reaction between lime and the cryptocrystalline alumina occurs at temperatures higher than ∼900 °C. This reaction involves the formation of transitory phases, $Ca_{12}Al_{14}O_{33}$ and $CaAl_4O_7$, at 916 °C and 1100 °C, respectively (Eqs. (5)–(11)). At temperatures higher than 1100 °C the intermediate phases, $Ca_{12}Al_{14}O_{33}$ and $CaAl_4O_7$, are completely disappeared and only $CaAl_2O_4$ was identified (as can be seen in Fig. 7b and Table 4).

As in the previous case, to support the reaction mechanism proposed thermodynamic calculations of the Gibbs energy ($\Delta G$) were used (Table 5). As in the above mentioned case, $\Delta G$ computations for the formation of $Ca_{12}Al_{14}O_{33}$, $CaAl_2O_4$ and $CaAl_4O_7$ confirm the much lower $\Delta G$ value for $Ca_{12}Al_{14}O_{33}$ in the whole range of temperatures considered. Consequently, its appearance as the first phase during the reaction of this sample is fully justified. These results are in good agreement with reported activation energies of different calcium aluminates,[25] the results obtained in $CaCO_3$/Al(OH)$_3$ mixtures at temperatures lower than 1000 °C by the authors[22] and higher than 1200 °C by Scian et al.[8]

Therefore, in both batches the solid state reactions between CaO and $Al_2O_3$ occur with the nucleation of transient phases such as CaO, $Ca_{12}Al_{14}O_{33}$, and $CaAl_4O_7$ at different points of the solid–solid interface. Further reaction occurs by

diffusion of reactant across the interface which depends of the particle size, mixing ratio and temperature.[22] According to the present data and the works of Ali et al.[21] and Singh et al.[9] the reaction happens by diffusion of the ion with the lower oxygen affinity, $Ca^{2+}$ into $Al_2O_3$.

Fig. 9a and b shows a scheme of the reaction mechanism. It may be explained in terms of the initial differences between the grain/agglomerate sizes of $CaCO_3$ and $Al_2O_3$. At temperatures ca. 900 °C, the larger $CaCO_3$ grains originate temporary porous CaO-segregations of 2–5 μm. The first formation of $Ca_{12}Al_{14}O_{33}$ occurs within the contacts between the small aggregates of lime and alumina particles and may produce domains of $CaAl_4O_7$ and, $Ca_{12}Al_{14}O_{33}$ of a few microns. In CAG and CA9 samples the presence of few microns agglomerates and either amorphous alumina or some scratches of alumina grinding media, respectively, may explain the formation of transitory $CaAl_4O_7$ domains. At higher temperatures $Ca^{2+}$ from aggregates would diffuse through $Ca_{12}Al_{14}O_{33}$ and $CaAl_4O_7$ layers to react and originate a homogeneous and porous single-phase $CaAl_2O_4$ as a final product.

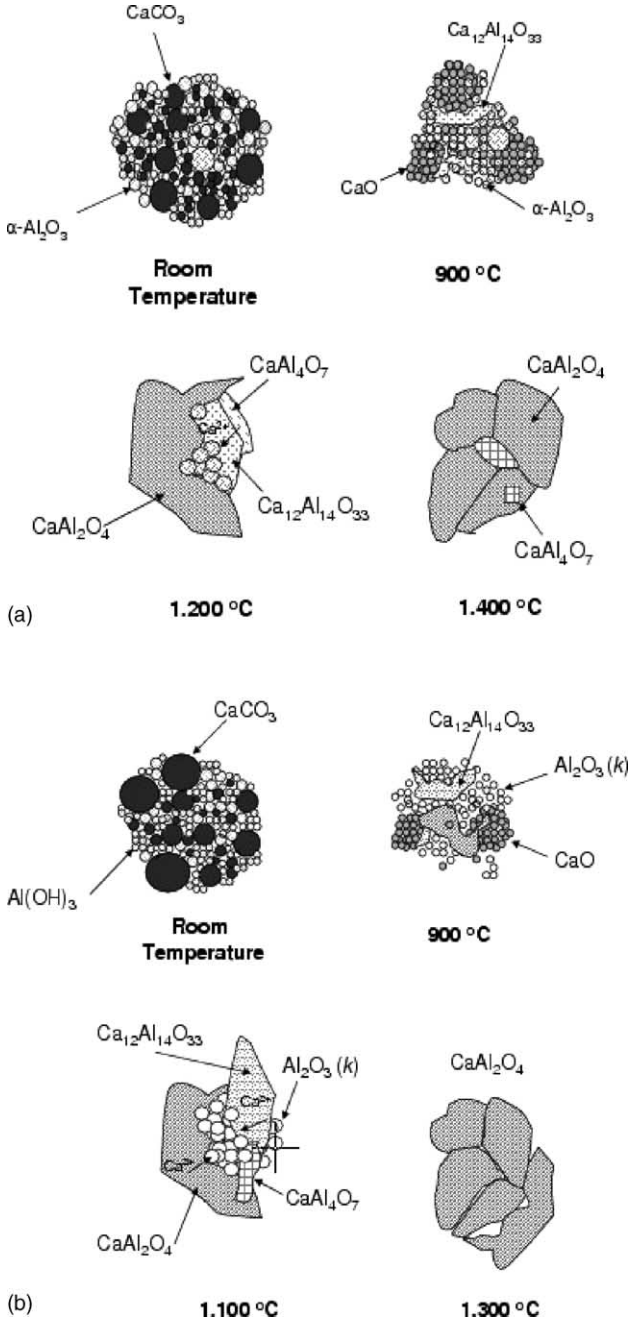


Fig. 9. Reaction mechanism sketch for the synthesis of $CaAl_2O_4$. (a) $CaCO_3$–α-$Al_2O_3$ mixture. (b) $CaCO_3$–$Al(OH)_3$ mixture.

All the mentioned reactions occur with large changes in volume. The loss of either $CO_2$ or $H_2O$ and the mentioned volume changes occurring during reaction disrupt the initial microstructure and create a network of new porosity (Figs. 6 and 7). The formed amorphous $Al_2O_3$ and CaO show a very small, nanometric crystalline size, which enhances the reactivity of the mixtures. In all the studied samples the reaction is finished at 1300 °C. Once the reaction is finished the densification begins. In the three samples the sintering process takes place at temperatures higher than 1250 °C.

### 4.2. Sintering process

The upper temperature limit for sintering (1400 °C) was established based on the CaO–$Al_2O_3$ phase diagram,[1] which exhibits a eutectic point at 1395 °C in the subsystem $CaAl_2O_4$–$Ca_{12}Al_{14}O_{33}$. Special care must be taken to avoid reaching the eutectic temperature since small deviations from the required stoichiometry can induce the development of undesired liquid phases in the vicinity of the $CaAl_2O_4$–$Ca_{12}Al_{14}O_{33}$ invariant point. Furthermore, in the CAG batch the presence of small sodium impurities in the aluminum hydroxide, <0.2 wt.% (Table 1), could provoke a significant temperature decrease from the ideal one.

In the case of the CA1 sample, it has to be mentioned that an expansive process occurs at 1400 °C (Fig. 3c). This can be explained keeping in mind the above mentioned $Al_2O_3$–CaO phase diagram. The average chemical composition of CA1 (Table 2) is located in the subsystem $Ca_{12}Al_{17}O_{33}$–$CaAl_2O_4$ whose eutectic point occurs at 1395 °C. Therefore, this expansive effect indicates formation of a liquid phase.

The presence of approximately 20% of liquid phase was detected at 1550 °C in CA1 sample by SEM (Fig. 8a). The small quantity of $Ca_{12}Al_{17}O_{33}$ detected by XRD corresponds to a phase that has been devitrified from the liquid phase during the cooling process of the sample.

Otherwise, sample CA9 has a solid state sintering up to 1550 °C but with the formation of small quantities of $CaAl_4O_7$. The formation of this phase is due to that the α-$Al_2O_3$ weight content in the CA composition (1) slightly increases with milling time, from 63.5 to 65.4%, due to the alumina release from the grinding media. In Fig. 6b it can be seen a fragment of alumina coming from the alumina balls wear. These observations indicate that very small differences in the stoichiometry of the composition, <2 wt.%, provide to the CA9 sample higher refractory characteristics with a temperature of first liquid formation of about 1600 °C.

Additionally, in sample CAG-30 the milling process was optimized by the use of high-purity magnesia partially stabilized zirconia balls (Mg-PSZ) as grinding media. In this case wear of the grinding media and secondary phases were not detected due to the better trybology of Mg-PSZ balls (Fig. 7a and b).

Bearing in mind the above mentioned results, the optimum thermal treatments for the samples studied were established at 1300 °C for CAG-30, 1350 °C for CA1 and 1400 °C for CA9 composition.

## 5. Conclusions

The synthesis of $CaAl_2O_4$ was conducted by reaction of mixtures of either $\alpha$-$Al_2O_3$ or amorphous ($Al(OH)_3$) with $CaCO_3$ by means of high energetic attrition milling of the reactants. The *optimum* thermal treatments for the batches studied were established at 1300 °C for CAG-30, 1350 °C for CA1 and 1400 °C for CA9 composition. Then, the synthesis of $CaAl_2O_4$ can be reached at lower temperatures starting from high energetic attrition milled mixtures that contain $Al(OH)_3$. These temperatures are lower than that required for the traditional solid state reaction process.

The sequence of reactions observed during the heating process is in agreement with thermodynamic calculations. Transient crystalline phases such as $Ca_{12}Al_{14}O_{33}$ and $CaAl_4O_7$ are clearly detected during the reaction sintering process resulting in the final formation of a finely grained $CaAl_2O_4$ material.

When high energy attrition mills are used it is mandatory to use high wear resistant grinding media to either avoid undesirable contamination or have the less harmful contamination of the sample. In the present case, a casual excess of $Al_2O_3$ with respect to the $CaAl_2O_4$ stoichiometry (~2 wt.% due to the alumina coming from the alumina balls wear) have a positive effect on the results and ensures that highly refractory material is obtained.

## Acknowledgements

This research was partially supported by CICYT under projects MAT-2000-0941 and MAT-2003-C2-08331-CO2-01. J.M. Rivas Mercury is indebted to the AECI for the concession of a fellowship.

## References

1. Hallstedt, B., Assessment of the CaO–$Al_2O_3$ system. *J. Am. Ceram. Soc.*, 1990, **73**, 15–23.
2. Toda, Y., Miyakawa, M. *et al.*, Thin film fabrication of nano-porous $12CaO{\cdot}7Al_2O_3$ crystal and its conversion into transparent conductive films by light illumination. *Thin Solid Films*, 2003, **445**, 309–312.
3. Lemonidou, A. A. and Vasalos, I. A., Preparation and evaluation of catalysts for the production of ethylene via steam cracking. Effect of operating conditions on the performance of 12CaO–$7Al_2O_3$ catalyst. *Appl. Catal.*, 1989, **54**(1), 119–138.
4. Singh, V. K., Sintering study of calcium aluminate. *J. Mater. Sci.*, 1996, **31**, 5163–5168.
5. Singh, V. K., Sintering of calcium aluminate mixtures. *Br. Ceram. Trans.*, 1999, **98**(4), 187–191.
6. Kraft, L. and Hendersson, L., Hardness and dimensional stability of a bioceramic dental filling material based on calcium aluminate cement. In *Proceedings of the 26th Annual Conference on Composite, Advanced Ceramics, Materials and Structure, Vol 23, No. B(4)*, ed. H. T. Lin and M. Singh, 2002, pp. 825–832.
7. Gotkas, A. A. and Weinberg, M. C., Preparation and crystallization of sol–gel calcia–alumina compositions. *J. Am. Ceram. Soc.*, 1991, **74**(5), 1066–1070.
8. Scian, A. N., Porto López, J. M. and Pereira, E., High alumina cements. Study of $CaO{\cdot}Al_2O_4$ formation stoichiometric mechanism. *Cem. Concr. Res.*, 1987, **17**, 198–204.
9. Singh, V. K., Ali, M. M. and Mandal, U. K., Formation kinetics of calcium aluminates. *J. Am. Ceram. Soc.*, 1990, **73**(4), 872–876.
10. Moore, R. E. and Sang, R. H., Chemical synthesis of monocalciun aluminate powders. *Bol. Soc. Esp. Ceram. Vidr.*, 1993, **32**(6), 369–376.
11. Gülgun, M. A., Popoola, O. O. and Kriven, W. M., Chemical synthesis and characterization of calcium aluminate powders. *J. Am. Ceram. Soc.*, 1994, **77**(2), 531–539.
12. Uysal, O. and Cúneyt, T. A. S. A., Chemical preparation of the binary compounds of CaO–$Al_2O_3$ system by combustion synthesis. In *Proceedings of the International Symposium of Innovative Processing and Synthesis*, 1997, p. 85.
13. Yi, H. C., Guigné, J. G., Moore, J. J. *et al.*, Preparation of calcium aluminate matrix composites by combustion synthesis. *J. Mater. Sci.*, 2002, **37**, 4537–4543.
14. Temuujin, J., Mackenzie, K. J. D. *et al.*, Effect of mechanochemical treatment on the synthesis of calcium dialuminate. *J. Mater. Chem.*, 2000, **10**, 1019–1023.
15. Senna, M., Incipient chemical interaction between fine particles under mechanical stress a feasibility of producing advanced materials via mechanochemical routes. *Solid State Ionics*, 1993, **63–65**, 3–9.
16. Cremer, W., Defined grinding in a grinding chamber former as an annular gap. *Interceram*, 1989, **5**, 59–61.
17. SSUB, SGTE substance database, Thermo-Calc Software version P, Stockhol Technology Park, Division of Computational Thermodynamics, Department of Materials Science and Engineering, Royal Institute of Technology, Stockholm, Sweden, 2003.
18. Kristóf-Makó, É. and Juhasz, A. Z., The effect of mechanical treatment on the crystal structure and thermal decomposition of dolomite. *Thermochim. Acta*, 1999, **342**(1/2), 105–114.
19. Carrizosa, I., Criado, J. M., García, F. G. and González, M., Influencia de las condiciones experimentales en la cinética de descomposición térmica de $CaCO_3$. *Bol. Soc. Esp. Ceram. Vidr.*, 1978, **17**(1), 23–27.
20. Singh, V. K. and Mandal, U. K., Kinetic study of the thermal synthesis of calcium dialuminate above 1400 °C. *Trans. J. Br. Ceram. Soc.*, 1982, **81**(4), 112–113.
21. Ali, M. M., Argawal, S. K. and Handii, S. K., Diffusion studies in formation and sintering of $CaAl_2O_4$ and $BaAl_2O_4$: a comparative evaluation. *Cem. Concr. Res.*, 1997, **27**(7), 979–982.
22. Rivas Mercury, J. M., De Aza, A. H., Turrillas, X. and Pena, P., The synthesis mechanism of $Ca_3Al_2O_6$ from soft mechanochemical activated precursors studied by time-resolved neutron diffraction up to 1000 °C. *J. Solid State Chem.*, 2004, **177**, 866–874.
23. De Aza, A. H., Pena, P., Rodriguez, M. A., Torrecillas, R. and De Aza, S., New spinel containing refractory cements. *J. Eur. Ceram. Soc.*, 2003, **23**(5), 737–744.
24. Guirado, F., Galí, S. and Chinchón, J. S., Thermal decomposition of hydrated alumina cement ($CAH_{10}$). *Cem. Concr. Res.*, 1998, **28**(3), 381–390.
25. Mohamed, B. M. and Sharp, J. H., Kinetics and mechanism of formation of tricalcium aluminate $Ca_3Al_2O_6$. *Thermochim. Acta*, 2002, **388**, 105–114.